Optical Code Division Multiple Access Devices and Systems

Daniel Pastor, Waldimar Amaya, José Capmany
Instituto de Telecomunicaciones y Aplicaciones Multimedia (iTEAM)
Universidad Politécnica de Valencia
Building 8G, access D, Camino de Vera s/n 46022 Valencia (SPAIN)
Corresponding author: dpastor@dcom.upv.es

Abstract

We present a summary of Optical Code Division Multiple Acces (OCDMA) Systems and Devices research activities developed at the Optical and Quantum Communications Group (OQCG).

Three main issues are covered; first we present a noise model of coherent DS-OCDMA systems where OOK and DPSK OCDMA modulation techniques are considered. The study includes synchronous and asynchronous assumptions and thresholding techniques. Secondly, we focus on the encoding–decoding efficiency versus wavelength detuning of the devices due thermal stability. Finally a new approach for the design of high reflectivity superstructured encoders and decoders is presented. This method uses Bragg gratings synthesis techniques to obtain the optimum devices profile which could be fabricated and tested for encoding and decoding.

Keywords: Fiber optics and optical communications, Multiplexing, Networks, Optical code division multiple access, Superstructured Fiber Bragg Gratings (SSFBG), DLP synthesis.

1. Introduction

Access networks are an important issue in present telecommunications infrastructures due to the increasing demand on capacity and diversity of services. Wavelength Division Multiplexing (WDM) and Electronic Time Domain Multiplexing (ETDM) are nowadays two consolidated technologies to face up the access segment requirements.

Despite this, Code Division Multiple Access (OCDMA) systems are a subject of constant research interest because it can be seem as a complementary technology in order to improve issues like flexibility, network safety, granularity and scalability amongst other [1-5]. The OCDMA system is represented in figure 1. Each digital source accessing the system is followed by an optical encoder that maps each information bit into a sequence of optical impulses or "chips" a long the bit period. This codification sequence can employ optical amplitude, phase or optical frequency variations between chips to imprint a specific and code-word assigned to each network user. The K users share the medium and the specific user information is extracted employing the proper optical decoder previous detection. Decoding accomplish the complementary optical process on the encoder. Encoding and decoding are performed optically, without electronic synchronization requirements, and the completed process should provide data signal recovery and Multi-User Interference (MUI) noise rejection. These all-optical features postulate OCDMA techniques to improve network security, on demand traffic flexibility, or spectral efficiency.

Encoding and decoding strategies can be grouped into Incoherent ones if the chip by chip differentiation is made attending only to amplitude/power of the lightwave and/or its optical frequency. In

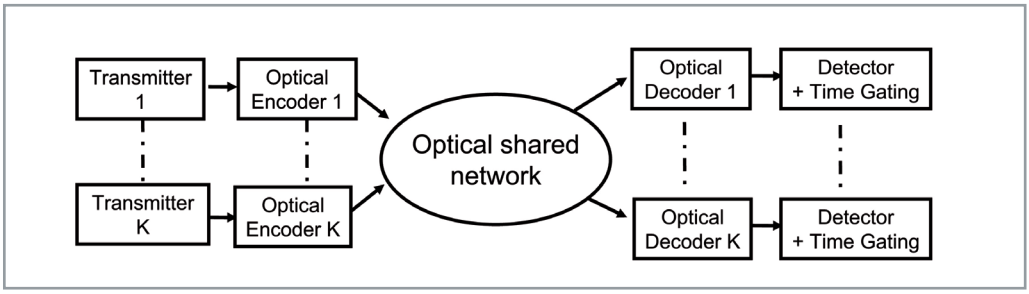

Figure 1. *OCDMA multi-user system diagram.*

these cases, optical phase does not play any rule in the en/decoding process. Figure 2 show a classification of OCDMA systems were Incoherent en/decoding can be divided into Time-Spread (TS), Frequency-Hopping (FH) and the more efficient combination of both the so called 2D-Time-Frequency coding [2, 6, 7]. Coherent techniques are whose employing the optical phase to apply the code-word in the encoding process and to reverse the process at the decoder. Figure 2 illustrates the two main coherent techniques. Spectral Phase Encoding (SPE) applies the optical phase changes according to a given code-word along the spectral components of the pulses to be codified [8]. The result is a time-spread signal that can be again reconstructed by conjugated spectral decoding. Coherent Time-Spreading (CTS) accomplish the optical phase encoding directly in the time domain regime imprinting relative optical phases to a set of different individual chips (delayed copies of the incoming pulse) according to the desired code-word [9]. Coherent techniques are considered more efficient than Incoherent ones in terms of code family correlation properties – very low cross-correlation among codes and high auto-correlation – because optical phase management take advantage of the adding and subtraction of electrical fields.

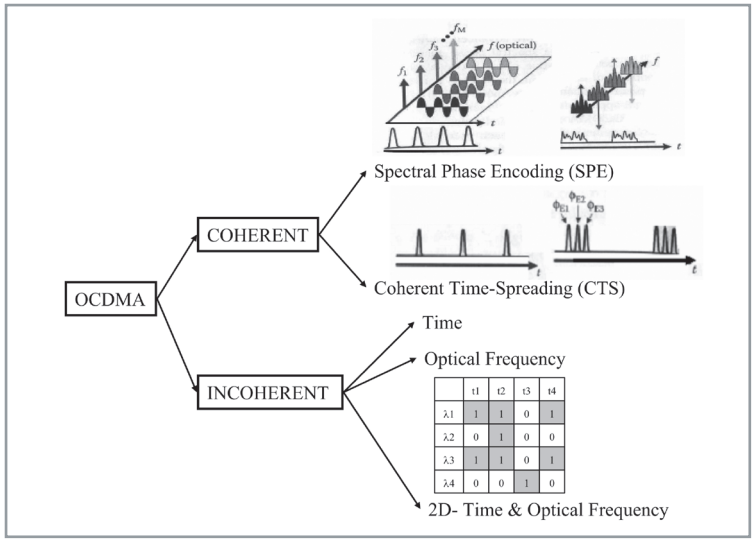

Figure 2. *OCDMA system classification.*

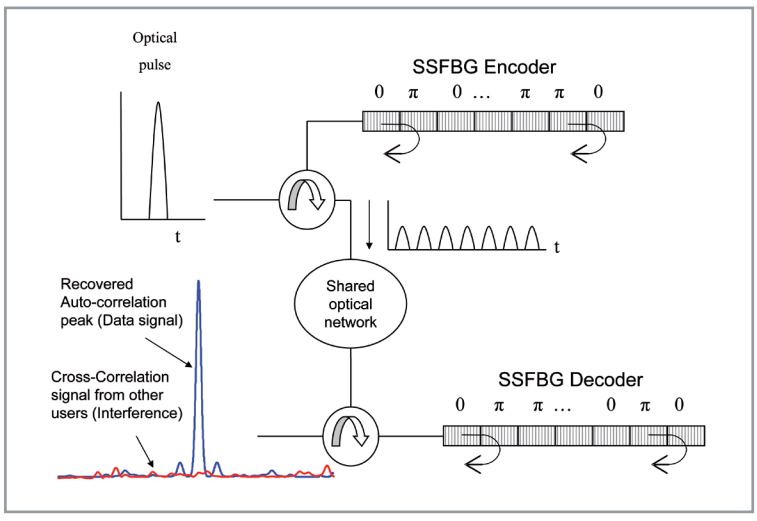

Figure 3. *Schematic structure of SSFBG in the en/decoding process.*

Many different technologies have been proposed to implement OCDMA systems. We can summarise them also attending to the classification on figure 2. Incoherent systems can exploit the spectral filtering characteristics of Array Waveguide Gratings (AWG) or Fibre Bragg Gratings (FBG) for both FH or 2D systems in combination with fibre delay lines [9 10]. Coherent systems require technologies were optical phase manipulation could be maintained stable and isolated from environmental changes. Moreover, this technology should allow the individual "chip" by "chip" phase control – or the individual spectral beam phase control in SPE . Planar Lightwave Circuits (PLC) and Super-Structured Fibre Bragg Gratings (SSFBG) are the two main technologies reported up to date to implement coherent systems. Early results in coherent Time-Spreading were reported employing PLC technologies based on optical splitting and combining structures interconnected with phase controllable delay lines [11], or more recently, employing specially designed PHASAR structures (like AWG structure) [5] or Ring Resonators combined with optical phase control to perform Coherent Spectral Phase Encoding [12].

Furthermore fiber based devices like the SSFBG have been proposed also [13] to perform coherent Time-Spreading OCDMA relaxing some relative drawbacks of PLCs like the long design and fabrication process, the non direct fibre compatibility that leads to insertion losses, etc. SSFBGs can be fabricated into the core of a standard single mode fibre by Ultra Violet (UV) light inscription [14]. The fabrication process can be made predictive and controllable in optical phase (as required by coherent coding) with moderate requirements on the fabrication premises. Figure 3 represent a pair encoder/decoder based on SSFBG. Each SSFBG can be described basically as a distributed reflection medium fabricated by imprinting along the device a periodic refractive index perturbation (generally of very low value). Amplitude, phase and period of the refractive index perturbation can be controlled along the device length during the fabrication process - this variation give the specific name of Super-Structured to the FBG. In figure 3, the applied pulse to the encoder is reflected back when it propagates inside the SSFBG. In this why, local amplitude and phase of the perturbation is mapped to the codified signal along the time axis providing coherent TS. The process is reversed at the SSFBG decoder by position rotation and optical phase conjugation of the encoder structure.

Following in this paper we present a summary of the research activities carried out by the authors in the context of Coherent Time-Spreading techniques employing Super-Structured Fibre Bragg Gratings at the Optical an Quantum Communication Group (OQCG). The summary is structured

into three parts: Time-Spreading OCDMA system modeling; SSFBG en/decoding wavelength detuning sensitivity; High reflectivity en/decoder design and fabrication.

2. Modeling of Time-Spreading OCDMA Systems

In this work area we have addressed the TS-OCDMA system modeling for the calculation of the different Multi-User Interference (MUI) noise sources and its impact over system Bit Error Rate (BER). Starting from a simple and intuitive model [15], we generalized it to describe arbitrary optical encoded/decoded chip shapes and electrical receiver responses. This modification is valid for all the systems with non perfect "time gating". Optical thresholding techniques are also discussed and included in the MUI noise power and eye opening calculations. Both On-Off Keying (OOK) and Differential Phase Shift Keying (DPSK) modulation and detection are also taken in consideration. Other important refinement of the model is the assumption of strict asynchronous multi-users interfering process in the decoder-receiver part of the system. We will exploit this asynchronous assumption when the chip time can be considered higher than the "chip width". It is in this case when clear statistical benefits are obtained reducing the dominant Primary Beat Noise (PBN). We provide a simple statistical model leading to highly intuitive Beat Noise term modifications to include this effect.

2.1 OCDMA system with On-Off Keying (OOK)

We start from the coherent TS-OCDMA model provided in [15], where we consider m active users out of a total of K users transmitting a bit "1" at a given time. We will assume total coherence for the optical signal beating (i.e., the coherence time of the different sources is higher than the chip time, $\tau c \geq Tc$). At this point, it is typical to assume "time gating" at the receiver and thus only accomplishing time integration along the chip time interval (Tc) around the peak of the decoded signal. This requires high speed electronics and/or non-linear optical processing making more complex and expensive the receiver but, nevertheless, being the straightforward way to reject the MUI noise contribution appearing along the whole bit period.

Fig. 4. shows schematically the 1 to m active interfering users perfectly overlapped with the properly decoded pulse and with constant power along the chip time. According with the previously outlined assumptions the detected signal can be written as [15]:

$$Z = \Re T_C \left(\begin{array}{l} P_d + \sum_{i=1}^{m} P_i + 2\sum_{i=1}^{m} \sqrt{P_i P_d}\, \cos(\Delta\Phi i) \\ + 2\sum_{i=1}^{m-1} \sum_{j=i+1}^{m} \sqrt{P_i P_j}\, \cos(\Delta\Phi_{ij}) \end{array} \right) \quad (1)$$

where P_d and P_i are the "data" decoded and the interfering power respectively, and $\Delta\Phi_i, \Delta\Phi_{ij}$ are the relative optical phases between the data and each interfering users and between different interfering users respectively. We can assume they are independent random variables uniformly distributed along the interval $[-\pi, \pi]$. From Eq. (1) we can clearly separate the different MUI noise contributions from the data signal as follows. The second term of Eq. (1) contains the sum of the power from

Each digital source accessing the system is followed by an optical encoder that maps each information bit into a sequence of optical impulses or "chips" a long the bit period.

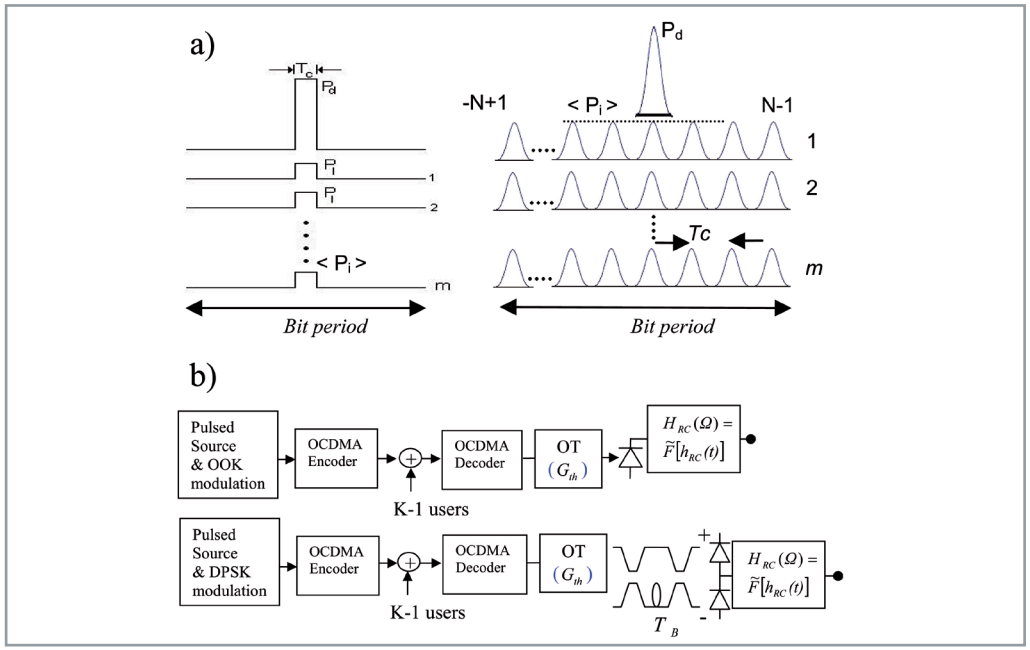

Figure 4. *a) (Left) Schematic TS-OCDMA system at [11]: Strict time gating along the chip time. m interfering users. (Rigth). Generalized model to include non perfect time gating and optical pulse shape. 2N-1 interfering chips from each untargeted user are considered inside the bit time, corresponding with code length N. b) System block diagrams for OOK and DPSK modulation.*

Planar Lightwave Circuits (PLC) and Super-Structured Fibre Bragg Gratings (SSFBG) are the two main technologies reported up to date to implement coherent systems.

the m interfering users. In a practical situation the P_i terms will not be a fix value but a random variable fluctuating around its average (P_i) according with the specific properties of the code employed. This term leads to a noise contribution that will be referred as Multiple Access Interference (MAI) and it will be quantified by the MAI power per one interfering user σ^2_{MAI-0}. A typical value for Gold Codes of 127 chips is $\sigma^2_{MAI-0}=6.5*10\text{-}5\ Pd^2$. The total MAI contribution will be for the m users:

$$\sigma^2_{MAI} = m\sigma^2_{MAI-0} \tag{2}$$

The third term of Eq. (1) represents the beating from each interfering user and the data. It will be present at the logical "1" and it represents the strongest contribution due to the beating with the data power. We will refer to it as Primary Beat Noise (PBN). If we define the crosstalk ratio at the encoding-decoding process as $\xi = \langle P_i \rangle / P_d$, and the previous assumptions for $\Delta\phi_i$, the PBN power is:

$$\sigma^2_{PBN} = 2\xi P_d^2 m \tag{3}$$

Finally the fourth term of Eq. (1) represents the mutual beating contribution between all the interfering users. This term will be referred as Secondary Beat Noise (SBN) and typically can be considered lower than the PBN. Like in Eq. (3) the SBN power is:

$$\sigma^2_{SBN} = \xi^2 P_d{}^2 m(m-1) \tag{4}$$

Up to this point, the model assumes a strong "time gating" restriction making flat time integration just only along the chip time. We have generalized the previous model to take into account an arbitrary receiver impulse response $h_{RC}(t)$ and optical coded and decoded pulse shape $s(t)$ [16].

Fig. 4 (right) represents schematically the properly decoded pulse of the data and the m interfering users signals at the decoder output distributed along the whole bit interval. In order to simplify the first expansion step we consider as in the previous model perfect overlapping between users.

The electric field complex envelop at the decoder output can be written as,

$$E(t) = s(t)\sqrt{P_d}\exp j(w_d t + \phi_d) + s(t) \otimes \left(\sum_{k=-(N-1)}^{N-1} \sum_{i=1}^{m} \left(\sqrt{P_i}\exp j\phi_{k,i}\right) \delta(t - kT_c) \right) \tag{5}$$

where Φ_{ki} is the relative optical phase for each chip at the decoder output along the bit period. Notice that the sum of chips extends up to 2N-1 terms which correspond to a code length N. As in the previous case, the noise power terms can be now rewritten as [16]:

$$\sigma^2_{PBN} = 2\mathrm{m}\xi P_d^2 \Gamma^2(0)$$
$$\sigma^2_{SBN} = m(m-1)\xi^2 P_d^2 \sum_{k=-(N-1)}^{N-1} \Gamma^2(-kT_c)$$
$$\sigma^2_{MAI} = m\sigma^2_{MAI-0} \sum_{k=-(N-1)}^{N-1} \Gamma^2(-kT_c) \tag{6}$$

where $\Gamma(t)$ function accounts for the receiver response and the optical pulses shape $\Gamma(t)=s^2 \otimes h_{RC}(t)$. For the bit error rate (BER) calculation we can assume Gaussian type probability density functions for the PBN and SBN if the number of interfering users m is higher then 4-5 [15]. Then we can employ the classical definition for the quality factor under Gaussian approximation and optimum threshold current $Q=(I_1\text{-}I_0)/\sigma_0+\sigma_1$ related with the BER by $BER(m)=1/2erfc(Q/\sqrt{2})$. Quality factor finally is given by [12],

$$Q_{OOK} = \left(\sqrt{\frac{m\overline{\Gamma}}{SNR_{MAI-0}} + m(m-1)\xi^2\overline{\Gamma} + \frac{1}{SNR_R}} + \sqrt{\frac{m\overline{\Gamma}}{SNR_{MAI-0}} + m(m-1)\xi^2\overline{\Gamma} + 2m\xi + \frac{1}{SNR_R}} \right)^{-1} \tag{7}$$

The whole OCDMA system BER for K total system users is calculated as the probability weighed sum of the all the cases from $m=0$ to $m=K\text{-}1$ active users as $BER = \sum_{m=0}^{K-1} p(m)BER(m)$, where $p(m)$ is the Binomial probability distribution, that is, the probability of m active users over K-1 total feasible interfering users. In expression (7) we use the normalized parameter $\overline{\Gamma}$ defined as,

$$\overline{\Gamma} = \left(\sum_{k=-(N-1)}^{N-1} \Gamma^2(-kT_c) \right) / \Gamma^2(0) \tag{8}$$

the MAI power per one interfering user σ^2_{MAI-0} is applied through the definition $SNR_{MAI-0}=P_d^2\sigma^2_{MAI-0}$ and the thermal and shot noise contributions at the receiver are both included in the definition of $SNR_R^{-1} = SNR_{th}^{-1} + SNR_{sh}^{-1}$, where the thermal and shot noise must be calculated as,

$$SNR_{th}^{-1} = \frac{N_{th}B_R}{\Re^2 P_d^2 \Gamma^2(0)}$$
$$SNR_{sh}^{-1} = \frac{2eB_R(1+m\xi)}{\Re P_d \Gamma^2(0)} \tag{9}$$

Being B_r the equivalent receiver bandwidth calculated over the receiver frequency transfer function $H_{RC}(\Omega) = \widetilde{F}[h_{RC}(t)]$, and N_{th} the thermal noise spectral density. Notice that the shot noise contribution as defined in Eq. (14) is applicable for the data symbol "1", and it could be neglected

for the "0" symbol or applied considering only $m\xi$ inside brackets.

We can already take some conclusions from Eqs. (8-9): 1) For low values of crosstalk level ξ the primary beat noise source is the dominant noise for a limited number a users. 2) Secondary Beat Noise increases with $m(m-1)\,\overline{\Gamma}$ and the incoherent MAI noise increases also with $m\overline{\Gamma}$. Lets consider here two extreme cases for the receiver bandwidth to quantify the $\overline{\Gamma}$ impact. First we consider the narrowest "time-gating", that is $B_R=1/2T_c$ (electrical bandwidths comparable to the chip rate). In this case we can assume $\Gamma^2(-kT_c)<<\Gamma^2(0)\forall k\neq 0$ and therefore $\overline{\Gamma}\approx 1$. Here the SBN and the MAI are the minimum feasible contribution. In the opposite extreme if the receiver bandwidth approach to the data bit rate $B_R\rightarrow 1/2T_b$, we can assume $\Gamma^2(-kT_c)\approx\Gamma^2(0)\ \forall k=[-(N-1),(N-1)]$ and therefore $\overline{\Gamma}\rightarrow(2N-1)$. Although this is an extreme case it indicates that the increase of SBN and MAI noise should be considered if the strict time gating condition is relaxed in a practical receiver. In an intermediate case, the parameter $\overline{\Gamma}$ integrate the 2N-1 chips contributing to the noise terms weighted by the $\Gamma(t)$ function. Notice that $\overline{\Gamma}$ can be considered as the effective number of chips contributing to SBN and MAI noise from 1 to the maximum 2N-1.

For completeness of the system model formulation, some insight have to be done into Optical Thresholding (OT) techniques. Different techniques have been proposed for the reduction of the MAI incoherent noise and the SBN exploiting optical power discrimination [8,17,19,20]. It is admitted also that optical thresholding techniques does not allow the reduction of PBN contribution.

Independently of the particular employed technology, optical thresholding can be included inside the system model if we consider an ideal "stepped power response" for the thresholder.

We define the optical gain due to the thresholding $(G_{th}=-10\log_{10}(g_{th}))$ as the optical power ratio at the thresholder output between the signal below and over the optical threshold. The modifications over the power noise terms at Eq. (8) and therefore over the Q factor at Eq. (7) affect in a different way depending if the symbols "0" or "1" are considered. They can be included easily substituting the original $\overline{\Gamma}$ by,

$$Bit\ '0'\rightarrow \overline{\Gamma}_0'=\overline{\Gamma}g_{th}^2$$
$$Bit\ '1'\rightarrow \overline{\Gamma}_1'=\left((\overline{\Gamma}-1)g_{th}^2\right)+1 \tag{10}$$

Notice that for symbol '0', SBN and MAI noises are reduced for all the equivalent number of chips $\overline{\Gamma}$, but on the "1" symbol the thresholding gain benefit only appear if $\overline{\Gamma}>1$. Eye opening I_1-I_0 at Q definition also will be affected by the thresholding gain,

$$I_1-I_0=P_d\Gamma(0)\left[1+\xi m\left(1-g_{th}\right)\right] \tag{11}$$

providing a result independent of $\overline{\Gamma}$. In order to include the thresholding effect into the model, $\overline{\Gamma}$ factor at Eq. (7) must be substituted bya $\overline{\Gamma}_0'$ or $\overline{\Gamma}_1'$ as Eq. (10) into the first (zeros) or second (ones) square root respectively, and the term $[1+\zeta m(1-g_{th})]$must appear now in the numerator.

2.2 OCDMA system with Differential Phase Shift Keying (DPSK)

Differential Phase Shift Keying (DPSK), has been proposed and demonstrated experimentally in OCDMA systems [20, 21]. It provides two mayor advantages: 1) Signal to noise and interference ration increases because symbol "0" provides additional energy and the eye opening increase in a factor two. 2) The eye opening after the differential detection provides symmetrical positive and negative values for "0" and "1" symbols leading into an optimum threshold detection level equal to zero independent of the average power incoming to the receiver. It reduces the complexity for threshold determination, but in other hand it requires additional devices like the differential detection and the optical Mach-Zehnder interferometer with one bit delay between arms. The system block diagram of fig. 4 represents the DPSK receiver structure after the OCDMA decoder. The signal and noise calculations for the DPSK-OCDMA system inherits all the previous OOK assumptions in terms of pulses shape, data signal and interference location and random phase variables. In DPSK case both data pulses and interference contribution now appear jointly with its correspondent interference contribution from the adjacent bit. Note that these interfering contributions from the same user are uncorrelated (different bits). We referee to [16] for a more detailed description of the DPSK model derivation where finally the noise terms can be written as,

$$\sigma_{PBN}^2=\frac{1}{2}\left(mP_d^2\xi\right)\Gamma^2(0)$$
$$\sigma^2{}_{SBN}=\frac{1}{2}\left(m(m-1)P_d^2\xi^2\right)\overline{\Gamma}\Gamma^2(0)$$
$$\sigma_{MAI}^2=m\left(\sigma_{MAI\_0}^2-(\xi P_d)^2\right)\overline{\Gamma}\Gamma^2(0) \tag{12}$$

The quality factor Q_{DPSK} is calculated with (12) taking account that now for DPSK I_1-$I_0=2P_d\Gamma(0)$ and $\sigma_0=\sigma_1$. Note that contrarily to OOK, in DPSK the dominant PBN noise term appears at both symbols, and also note that the eye diagram amplitude is not affected by the average MAI contribution to photocurrent. Finally Q_{DPSK} is

$$Q_{DPSK}=\left(\sqrt{m\left(\frac{1}{SNR_{MAI-0}}-\xi^2\right)\overline{\Gamma}+\frac{1}{2}m(m-1)\xi^2\overline{\Gamma}+\frac{1}{2}m\xi+\frac{1}{SNR_R}}\right)^{-1} \tag{13}$$

In (13) we employ $\bar{\Gamma}$ as defined in (8), but also in the case that Optical Thresholding could be employed before the DPSK receiver $\bar{\Gamma}$ should be modified as in (10) but only attending to the "1" symbol case, and without any modification of eye opening I_1-I_0. We can compare expressions (7) and (13) with the same eye opening (i.e. both expressions normalized with numerator equal to 1). We can point out: 1) If PBN can be considered the dominant noise term them $Q_{DPSK}/Q_{OOK}=2$ or the feasible m interfering users increase in a factor 4. The same result is obtained if the thermal noise should be dominant. 2) If $m>>1$ and $\bar{\Gamma}>>1$ and the SBN could be not negligible we have $Q_{DPSK}/Q_{OOK}=2\sqrt{2}$.

The complete OCDMA system comparison between OOK and DPSK modulation must be evaluated by means the system BER, but now for OCDMA-DPSK $BER_{DPSK}=BER_{DPSKa}(m=K-1)$ and

for OOK $BER_{OOK}=\sum_{m=0}^{K-1}p(m)BER_{OOK}(m)$ as described. In DPSK all the K users are "active" for all the transmitted bits, and the total BER is not weighed by any statistical averaging.

2.3 OCDMA system numerical performance evaluation.

For the system performance evaluation we have fixed the BER to 1e-9 and we have obtained the maximum allowed system users K versus the crosstalk level. We take into account both OOK and DPSK modulations, but also the cases were time gating conditions are perfect or non-perfect (as described in previous section), and the Optical Thresholding (OT) is employed or not. As expected, DPSK modulation provides better results increasing the number of feasible users approximately in a factor 4 [20]. This improvement is slightly reduced when the number of users is high because the statistic averaging of the OOK system is affecting. Traces labeled as (a) in Fig. 5 represents the perfect time gating case $\bar{\Gamma}=1$ $(B_R=1/2T_c)$ and the traces (b) are calculated considering that 5% of the interfering chips per bit are acceding to the detector o equivalently that our electrical bandwidth is limited to $B_R=(1/2T_c)\bar{\Gamma}=(1/2T_c)(2N-1)(5/100)$. This slight reduction of time gating quality impacts strongly over the system performance decreasing the maximum allowed users in a factor of approx. 2. In this conditions SBN and MAI are not negligible terms. Finally traces (c) depict the improvement that Optical Thresholding provides just only with an optical gain of 5 dB as reported in [19-20], due to the power reduction of the interfering signals embraced in SBN and MAI. Higher optical thresholding gains makes traces (c) converge to (a).

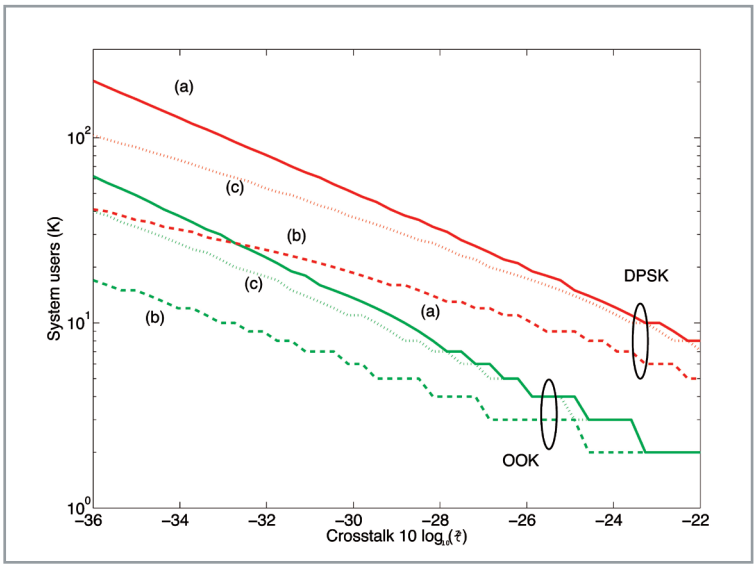

Figure 5. *OCDMA system performance comparison for OOK and DPSK modulation. BER is fixed to 1e-9. a) Perfect time gating covering only the chip time ($\bar{\Gamma}=1$). b) Nonperfect time gating covering the 5% of the total interfering chips per bit. c) Non-perfect gating like (b) but employing Optical Thresholding with $G_{th}=5dB$.*

2.4 Primary Beat Noise Reduction under Asynchronous Hypothesis.

Primary Beat Noise is the dominant multi-user interference noise term. It is directly proportional to the crosstalk level ζ versus the Secondary term that is proportional to ζ^2. When the total number of users K increases, lower values of crosstalk ζ are required to maintain the specified system BER. As it will be detailed later, in a system with K=5 users, the crosstalk level $(10log_{10}(\zeta))$ should be lower than -30 dB to ensure a power penalty under 1 dB due to MUI. For coherent TS-OCDMA codes, the crosstalk level can be approximated in the better fabrication case to $\zeta \approx 1/N$ where N is the code length or number of chips per bit. For the $K=5$ example the code length should be N>1000, that represents a value higher to the nowadays maximum reported code length N=512 (for example at [13]).

Previous calculation take the simplifying assumption that all the m interfering chips overlap perfectly with the decoded data pulse (see Fig. 4). Although this assumption reduces the model complexity and it represents the worse system scenery, it is also a very improbable case in a real network under asynchronous assumption. Asynchronous overlapping between signal and interference will improve the system performance when the chip time T_c defined as the time between two adjacent code chips would be higher than the own chip duration σ_c (see Fig. 6 (left)).

In order to quantify the PBN reduction under asynchronous case we will assume the following simplifications:

1) L discrete positions are defined along the chip time spacing (T_c), where the m interfering chips can allocate randomly. We will refer to these discrete positions as slots. We assume that the occupation probability of each time slot by one interfering user is uniformly distributed along the slots, so with probability. $\alpha=1/L$

2) The chip time width (σ_c) is equal for all users and it is given by $\sigma_c=T_c/L$. We will also neglect the overlapping between adjacent chips.

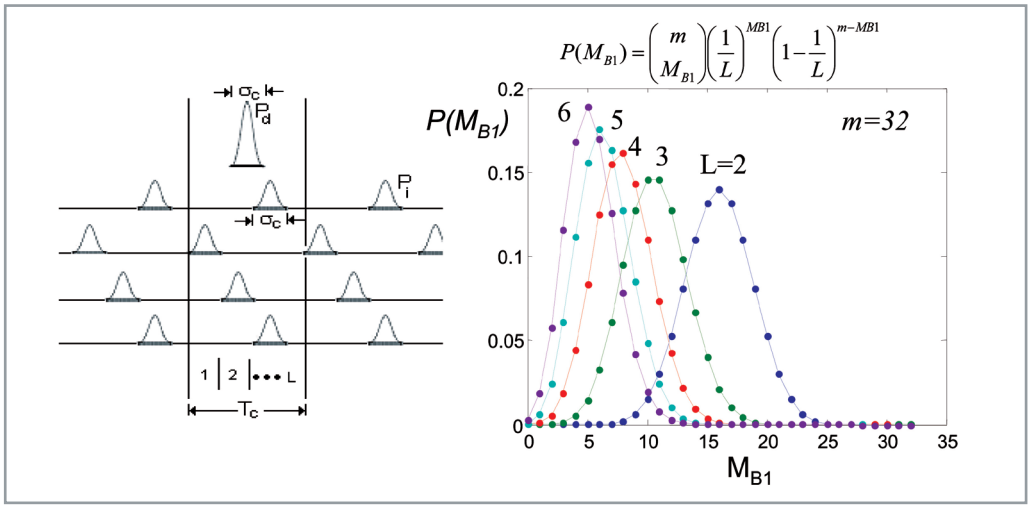

The non perfect overlapping between signal and interference under the asynchronous assumptions provides clear statistics benefits to the overall TS-OCDMA system.

Figure 6. (Left) Asynchronous TS-OCDMA system scenery. Interfering signals does not overlap perfectly with decoded data signal (Pd). (Rigth) Probability distribution function of MB1 interfering chips overlapping the data chip.

3) M_{B1} is defined as the number of interfering users from the total m set, that actually go to the same slot where the data recovered signal (P_d) goes. These M_{B1} chips contribute to PBN.

4) $M_{B2}(l)$ is a vector containing the number of interfering users from the remaining m-M_{B1} set, that they go to the slot number l with $l \in [1 \rightarrow (L-1)]$. They produce SBN. M_{B1} and $M_{B2}(l)$ embrace the whole m interfering user as

$$M_{B1} + \sum M_{B2}(l) = m.$$

Under this system model extension, different feasible combinations of M_{B1} and $M_{B2}(1)$ produce different PBN and SBN power values, and therefore a different system BER. Moreover the probability of occurrence of the different combinations of M_{B1} and $M_{B2}(1)$ expands over a broad dissimilar values, weighting the whole system BER as

$$BER(m) = \sum P(M_{B1}, M_{B2}) \cdot BER\,(M_{B1}, M_{B2}) \tag{14}$$

where $P(M_{B1}, M_{B2}(l))$ is the particular combination probability. Now the noise power terms can be rewritten [16] to include the M_{B1} and $M_{B2}(l)$ splitting of the whole a interferening users as,

$$\sigma^2_{PBN} = 2 M_{B1} \xi P_d^2 \Gamma^2(0)$$

$$\sigma^2_{SBN} = \xi^2 P_d^2 \sum_{k=-N}^{N-1} \Gamma^2(-kT_c) \left[M_{B1}(M_{B1}-1) + \sum_{l=1}^{L-1} \left(M_{B2}(l)(M_{B2}(l)-1) \right) \right] \tag{15}$$

We have assumed that the m-$MB1$ interfering users causing the SBN are uniformly distributed along the $l \in [1 \rightarrow (L-1)]$ positions in order to simplify the calculations of the total BER (see [16]).

The overall TS-OCDMA system performance evaluation will be carried out employing the Multi-User Interference (MUI) penalty. We define it as the required increase of averaged optical power at the receiver input, respect to the thermal noise limited case, to compensate the MUI degradation and therefore to maintain a certain BER figure. The statistic benefits of the asynchronous model $(L>1)$ can be summarized into Fig. 7 where we represent the relationships between K, L and Crosstalk, fixed the maximum penalty due MUI noise to 1dB. From the results with $(L=1)$ we can see the strong reduction required on the crosstalk if the number of users K increase, making the system not feasible. The increase of L just to $L=2$ or $L=4$ expands the number of feasible system users. The improvements in the number of users K when L is increased is more emphasized for lower crosstalk values. If the crosstalk is ~ $-29dB$, $L=2$ provide K=5 users, L=4 provides K=8 and L=10 provides only K=13, but if crosstalk reach -33 dB the achievable number of users for L=1, 2, 4 and 10 reach K=7, 14, 21 and 30 respectively.

The non perfect overlapping between signal and interference under the asynchronous assumptions provides clear statistics benefits to the overall TS-OCDMA system. But also it requires to pay a price in other system aspects. If we want to increase the ratio L maintaining the code length N, we have two alternatives: 1) Reduction of the pulse width σ_c if the chip time is fixed. Mode-Locked pulsed lasers based on fiber rings are commercially available providing pulse width between 0.1 and 1 ps. This will produce an increase of the occupied optical spectrum by a factor L, and additionally such a sources could be not cheap enough to mach with the low cost expected per user. 2) To increase the chip time maintaining the pulse width. In this case, if we want to maintain the crosstalk level the number of chips N should be maintained and therefore the bit rate per user should be reduced in the factor L. Let us consider an example: σ_c=0.5 ps (~16 nm spectral bandwidth), code length is N=511 chips $(\zeta(dB)=-27)$. The maximum chip time is given by $T_C \approx T_B/2N$, so for 622Mb/s per user we

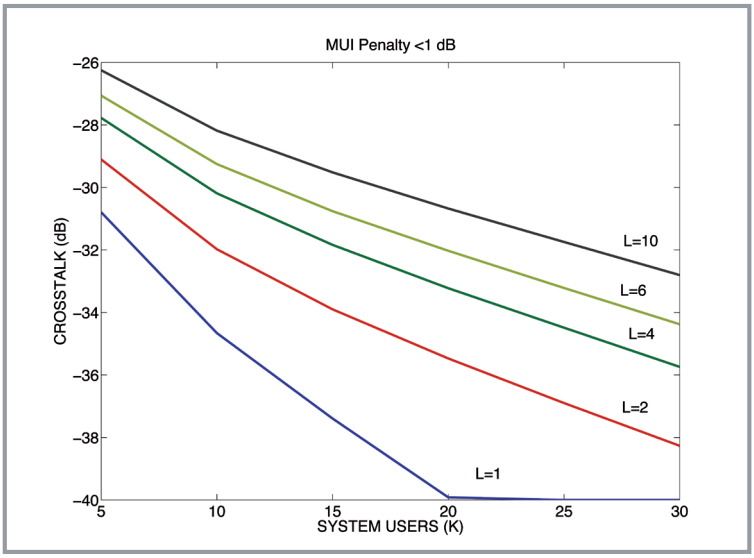

Figure 7. *Maximum allowed Crosstalk (10log10(ξ)) v.s. the number of users (K). Curves correspond with different values of L ratio ($L=T_c/\sigma_c$) for the asynchronous model.*

have a $L \sim 3$ and for 155 Mb/s $L \sim 12$. In any case, although values of L >3-4 seems to be difficult to achieve in the practice without sacrifice optical frequency bandwidth it must be understand like an additional degree of freedom for the time-frequency multiplexing map of the OCDMA system.

3. SSFBG en/decoding wavelength detuning sensitivity

We address the degradation effects induced by the optical wavelength detuning between encoder and decoder devices, providing a simple theoretical model for the vanishing of the autocorrelation peak. The model was verified experimentally for two different total length encoder–decoder pairs of 63 chip gold sequence code word with binary phase encoding at 104 and 174 Gchip/s chip rates. Moreover, the vanishing effect has been proposed as an additional degree of multiplexing allowing code-word reutilization and/or code "tuning" facility employing the same physical SSFBG device.

3.1 En /Decoding Efficiency model.

We consider a SSFBG device composed of N fiber sections or "chips" spaced lch along the fiber. We also assume as the general case an "in-phase" coded system, where C_a represents the complex amplitude and phase associated with the local reflectivity on each chip section. The electric field complex envelope impulsive response for the SSFBG structure is:

$$h_{co}(t)=\sum_{i=1}^{N} C_i h_{ch}(t-(i-1)t_{ch})\exp\left[j2(i-1)l_{ch}\beta(\lambda)\right] \tag{1}$$

where $h_{ch}(t)$ an be defined as the normalized impulsive response of a single chip. $t_{ch}=2l_{ch}/v_g$ is the chip time, and $\beta(\lambda)$ is the propagation constant into the SSFBG at the applied wavelength. From the argument of the exponential function in (1) we can derive an important design condition for the round trip optical path $(2l_{ch})$ between two chips. It should produce only integer jumps of 2π phase to ensure the proper coding and decoding, and the design rule from (1) is:

$$l_{ch}=\frac{\lambda_B}{2\bar{n}}q \tag{2}$$

being q an integer, λ_B the Bragg wavelength and $\bar{n}$ the effective refractive index of the mode. Condition (2) ensures a zero incremental optical phase from one to other chip along the code when a wavelength signal λ_B is applied to the device. If we apply any other wavelength $\lambda=\lambda_B+\Delta\lambda$, from (1) and (2) the encoded response will result into:

$$h_{co}(t)=\sum_{i=1}^{N} C_i h_{ch}(t-(i-1)t_{ch})\exp\left[j(i-1)2\pi q\left(1-\frac{\Delta\lambda}{\lambda_B+\Delta\lambda}\right)\right] \tag{3}$$

If we define $\Delta\Phi=-2\pi q(\Delta\lambda/(\lambda_B+\Delta\lambda))\approx-2\pi q(\Delta\lambda/\lambda_d)$, encoder and decoder responses can be written respectively as

$$h_{co}(t)=\sum_{i=1}^{N} C_i h_{ch}(t-(i-1)t_{ch})\exp\left[j(i-1)(2\pi q+\Delta\phi_{co})\right] \tag{4}$$

$$h_{deco}(t)=\sum_{k=1}^{N} C^*_{N-k+1} h_{ch}(t-(k-1)t_{ch})\exp\left[j(k-1)(2\pi q'+\Delta\phi_{deco})\right] \tag{5}$$

where we have employed for the decoder the conjugated and time inverted code word $C_{decorer(k)}=C^*_{coder}(N-k+1)$, the same individual chip response and chip space a as the standard procedure. After decoder, the signal can be obtain by time convolution of (4) and (5), and the autocorrelation peak can be expressed as the following summation:

$$\left(h_{co}\otimes h_{deco}\right)\Big|_{t=(N+1)t_{ch}} = h_{ch}(0)\exp\left(jN\Delta\phi_{deco}\right)\sum_{i=1}^{N}\left(C_i C^*_{N-i+1}\right)\exp\left\{j(i-1)(\Delta\phi_{co}-\Delta\phi_{deco})\right\} \tag{6}$$

Notice that the coder-decoder sequence design ensure $C_i C^*_{N-i+1}=1$.

From (6) we can obtain some conclusions. In the case of null wavelength detuning of both de encoder and decoder devices, the summation into (6) provides maximum value of N. That is, the perfect construction of the autocorrelation peak from the N codified chips. The autocorrelation peak construction will be also the maximum if the incremental phases are the same $\Delta\Phi_{co}-\Delta\Phi_{deco}=0$. This is the case when the two devices (coder and decoder) provide the same central wavelength $(\lambda_B|_{co}=\lambda_B|_{deco}=\lambda_B)$, and the pulsed source provides different central wavelength

$(\lambda=\lambda_B+\Delta\lambda)$. In this situation, the progressive chip to chip diphase along the coder is perfectly compensated along the decoder. Any other case with $\Delta\Phi co-\Delta\Phi deco\neq 0$ repraesents a real difference between the central operation wavelength of the devices. From (6) we can define the autocorrelation efficiency in terms of power as:

$$\eta=\left|\frac{\sum_{i=1}^{N}\exp\{j(i-1)(\Delta\phi_{co}-\Delta\phi_{deco})\}}{N}\right|^2=\left(\frac{\sin\left(\frac{N\Delta\phi_{co/deco}}{2}\right)}{\left(\frac{N\Delta\phi_{co/deco}}{2}\right)}\right)^2 \quad (7)$$

where the incremental phase difference between coder and decoder is referred as $\Delta\Phi_{co/deco}=\Delta\Phi_{co}-\Delta\Phi_{deco}\approx 2\pi q(\lambda_B|_{co}-\lambda_B|_{deco})/\lambda$. The efficiency given in (7) decrease strongly if the argument $(N\Delta\Phi/2)$ move away from zero, being zero if $N\Delta\Phi=2\pi$. The power penalty can be defined as $\delta=-10log10(\eta)$ and the limit of 1 dB power penalty $(\eta=0.8)$ from (7) corresponds with $N\Delta\Phi=1.62$. Applying this penalty limit and substituting the definition of q, we obtain the following condition for the maximum allowed detuning:

$$\left(\frac{\Delta\lambda_B}{\lambda}\right)\leq 1.62\frac{\lambda_B}{4\pi\bar{n}}\frac{1}{Nl_{ch}} \quad (8)$$

Notice that the maximum wavelength detuning is inversely proaportional to the total coder or decoder length (Nl_{ch}) [22].

3.2 Experimental Verification of Detuning Effects.

To quantify experimentally the wavelength detuning impact we have fabricated two pairs of encoder–decoder sets based on the same code word from the 63 chip gold sequence family with binary phase encoding, similar to [23]. The two pairs (encoder –decoder) differ only on the chip separations of lch=1 mm and 0.6 mm, corresponding to chip rates of 104 and 174 Gchips/s, respectively. Both SSFBG devices are centred at 1538 nm. After fabrication, the encoder and decoder from each pair were placed into respective electronically controlled thermal boxes. This provides thermal stability with 0.1°C accuracy and makes it feasible to tune the wavelength by temperature control to achieve the required device agreement. The encoding and decoding experiment was carried out employing a pulsed mode-locked laser source providing 2.5 ps width pulses at 1.25 GHz pulse rate. The encoded pulses expand along 604 ps (1 mm chip) and 361 ps (0.6 mm chip), respectively.

The inset of Fig. 8 shows the encoded sequence and the decoded autocorrelation peak. This properly decoded signal corresponds to the case of good wavelength agreement, producing a clear autocorrelation peak and low satellite "wings", but this situation vanishes rapidly if a slight wavelength detuning of just a few picometers is produced. The traces in Fig. 8 show the normalized autocorrelation peak power obtained experimentally and the theoretical efficiency for the two chip rate pairs (1 and 0.6 mm chip spacing), showing good agreement. The horizontal axis is the relative detuning provided by the thermal boxes, where the encoder was maintained at a fixed temperature and the decoder was changed progressively. The measured SSFBG wavelength versus temperature slope was $\sim 11\ pm/°C$ (unpackaged fiber). For a 1 mm chip length x 63 chips $(Nlch=63\ mm)$, the efficiency reduces to 50% for ±6 pm (±0.54°C for unpackaged fiber). For a 0.6 mm chip x 63 chips=37.8 mm, 50% reduction is reached at ±10 pm (±0.9°C). The maximum allowed detuning increases when the product $Nlch$ decreases, although this possibility is limited technologically by the minimum achievable chip length and by the necessity of longer code words (N) to reduce the multiple access interference (MAI) and beat noise. Applying Eq. (8) to some examples of large chip numbers, $N=255$ or 511 at 320 Gchips/s, that were already reported [13, 24], we obtain 1 dB penalty limits of $\Delta\lambda B$=1.6 pm and $\Delta\lambda B=0.8\ pm$, respectively.

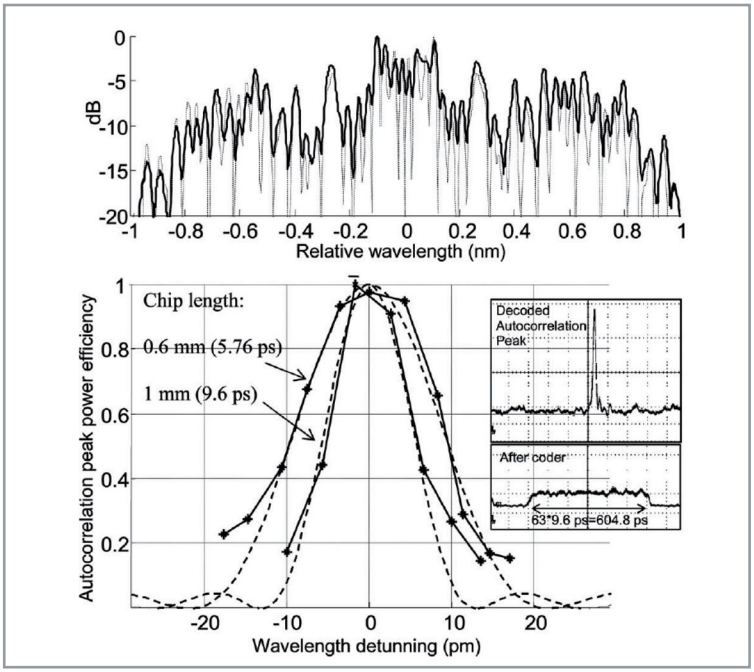

Figure 8. *Upper part: measured and calculated optical spectra of the SSFBG encoder–decoder (N=63, gold sequence, 0.6 mm chip length). Lower part: normalized autocorrelation peak power efficiency. Measured and theoretical model. Inset: example of encoded and decoded signal.*

Despite the previous considerations, autocorrelation peak erasing can be employed also as an additional degree of multiplexing just by modifying slightly the relative wavelength position between the encoders and decoders. To verify this possibility experimentally we assembled three identical coders based on the same 63 chip gold sequence (C1) (at 174 Gchips/s) at three different temperatures employing thermal stabilizing boxes. The three encoders were wavelength spaced by only ~50 pm. The matched optical fil-

We have proposed a complete compensation approach based on the use of FBG synthesis techniques to find the specific refraction index perturbation profile that ideally provides the flat expected impulse response for the encoder and decoder.

ter (reversed device), was tuned along the wavelength span through the three transmitters.

Figure 9 shows the autocorrelation peaks obtained when the decoder is tuned at each coder wavelength, and also the spread signal without peak obtained from the other two non-wavelength-matched coders in each case. Measurements were obtained by direct detection with a 30 GHz bandwidth optical sampling scope. These time measures were taken systematically along the wavelength axis to explore MAI.

Figure 10 shows the maximum peak-to-peak power decoded at the receiver along the complete 800 ps time period for the three consecutively connected coders (transmitters). Notice that mutual interference remains bounded in a 20%–25% band along the wavelength detuning axis. The reported value was similar to that obtained decoding at the receiver with an orthogonal code word (C2) from the same N=63 gold sequence set (see code 2 in [23]).

4. Design of High Reflectivity Superstructured FBG for Coherent OCDMA

FIn coherent DS-OCDMA (also referred to as time-spreading OCDMA) each bit of information is encoded into a great number of short pulses or 'chips' along the original data bit period. In the coherent approach, chips are phase modulated in a binary or quaternary [24] pattern according to a properly designed codeword family (for example M-sequences or Gold codes). At the decoder end, before electrical detection, the original pulse is reconstructed employing the time-reversed codeword with conjugated phases. Note that the proper rejection level between orthogonal codewords (referred as cross-correlation or interference signal) will be a key aspect in multi-user systems, and it depends on the code family, but generally it is improved as the chip number N increases. There are two main technologies widely demonstrated in the literature for coherent DS-OCDMA: planar lightwave circuits (PLC) [5], and superstructured fibre Bragg gratings (SSFBG) [23-25], and we address in this Letter the design aspects for the latter technology. In SSFBG-based coding a short pulse is applied to a specially designed FBG with constant amplitude index perturbation and modulation of the local Bragg phase. The reflected impulsive response maps onto the time response the optical phase changes imprinted along the SSFBG. Local reflectivity amplitude must be maintained weak enough to allow the pulse to propagate along the whole SSFBG without significant power depletion and free of distortion due to multiple reflections. SSFBG en/decoders are inexpensive, fibre compatible devices, and they have been fabricated with a great number of chips (up to N=511 [5]). Despite this, weak reflectivity SSFBG en/decoders present strong insertion losses *(>10 dB)* [25] to preserve good encoding and decoding capabilities and therefore low cross-correlation signals between orthogonal codewords. In [25] has been proposed a heuristic apodisation function along the SSFBG local reflectivity to compensate for the power depletion and to be able to increase the local reflectivity. This provides a reduction of the insertion losses but it does not address the distortion on the impulsive response of en/decoders produced by multiple reflections. In this framework we have proposed [26] a complete compensation approach based on the use of well known FBG synthesis techniques [27] to find the specific refraction index perturbation profile that ideally provides the flat expected impulse response for the encoder and decoder. This is an integral approach that provides power depletion and multiple reflection compensation for high reflective SSFBGs.

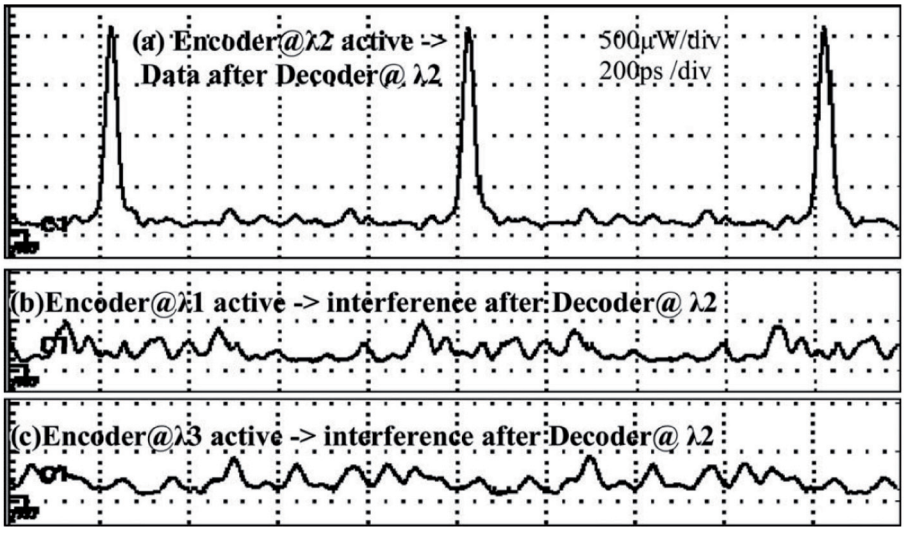

Figure 9. *Decoded signal by receiver with decoder tuned to λ2 proceeding from three different transmitters: (a) transmitterat λ2 active, (b) transmitter at λ1 active, (c) transmitter at λ3 active.*

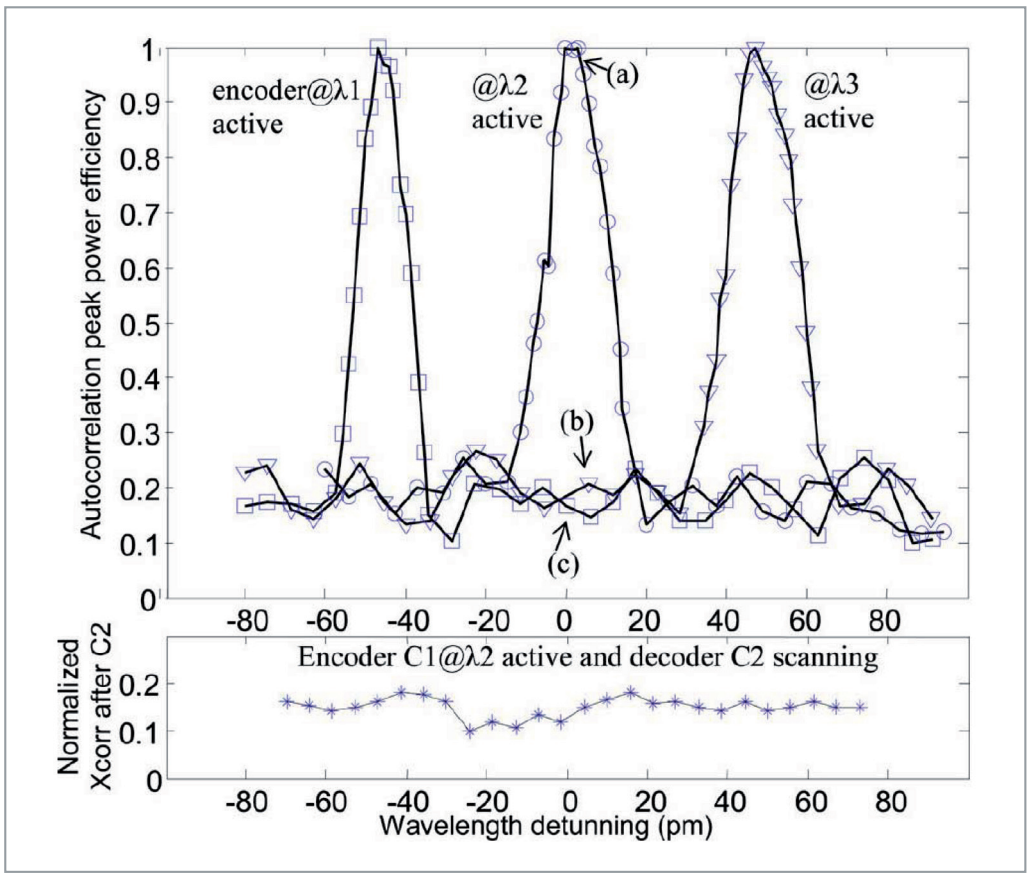

Figure 10. *Normalized maximum peak-to-peak power detected after decoder scanning in wavelength. Transmitters at λ1, λ2, and λ3 (spaced _50 pm) were activated consecutively. (a), (b), and (c) correspond to the scopes in Fig. 9. Lower part: normalized cross correlation between C1 and C2 when detuning C2 decoder.*

4.1 Design proposal and experimental verification

The design process that we propose inverts the standard approach employed for weak SSFBGs. On the standard one, the selected codeword containing the binary or quaternary phase modulated chips is mapped onto complex coupling coefficient $q(z)= |q(z)|exp\ (j\varphi(z))$ [cm_1] (proportional to the refractive index perturbation profile $\Delta n(z))$, where $|q(z)|$ is constant, and $\varphi(z)$ contains the phase changes dictated by the codeword at the proper chip positions. The sequence can be summarised as: codeword → construction of $\varphi(z)$ with $|q(z)|=constant$ → resultant device with non-ideal impulsive response $h(t)$. In this process if we try to increase $|\Delta n|> 7x10^{-5}$ (high reflective gratings) [25], the resultant $h(t)$ will be seriously damaged owing to p ower depletion and multiple reflections. We propose to invert the process by fixing the ideal objective impulsive response $h(t)$ for the device and to find by a synthesis method the specific complex coefficient profile that provides such a $h(t)$. In this case the sequence is: codeword → expected $h(t)$ construction with the required peak reflectivity → synthesis method to obtain $q(z)$. To verify the process we applied it to a 63-chip codeword (C1) from a Gold code family as in [23]. To construct the objective $h(t)$ response the system parameters were: chip time of 5.74 ps (174 Gchip=s), chip width 3 ps to avoid inter-chip erasing, and we supposed Gaussian chip shape. Finally, chip-to-chip amplitudes were constant and adjusted to provide the required peak reflectivity evaluating $R(w)= |FT\ [h(t)]\ |^2$.

Fig. 11a shows the $q(z)[C1]$ function obtained for the C1 code employing the discrete layer peeling (DLP) synthesis method by Skaar [27]. Note that the synthesis process has to be replicated for the decoder taking the codeword information in the opposite direction and conjugated phases leading to a different $q(z)$ profile. To verify the synthesised profile, we employ numerical coupled wave equation (CWE) analysis to obtain the reflection coefficient of $q(z)[C1]$ and finally the impulse response ($h(t)[C1]$) by inverse Fourier transform of it. The result is shown in Fig. 11b. From Fig. 11a we can see how the synthesised profile integrates at each step (each discrete chip) the required amplitude and phase to compensate for the power depletion suffered up to that point and all the spurious multiple reflections falling at that position from the remaining SSFBG structure. Synthesised $q(z)[C1]$ profile overpasses even the original code duration or size (i.e. 63x0.6 mm=37.8 mm) trying to compensate also for multiple reflection falling within this range. The synthesised $q(z)[C1]$ profile was fabricated employing a chip-by-chip illuminating process with accurate Bragg phase control. The approximately Gaussian UV beam was focused to ~350 mm and the chip-by-chip spacing was

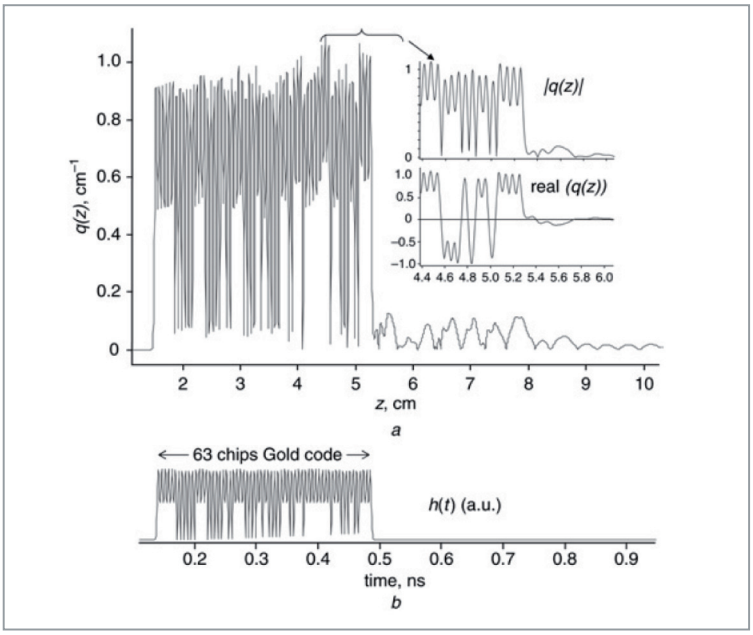

Figure 11. *Coupling coefficient of synthesised SSFBG by DLP and impulsive response of synthesised SSFBG (modulus)*

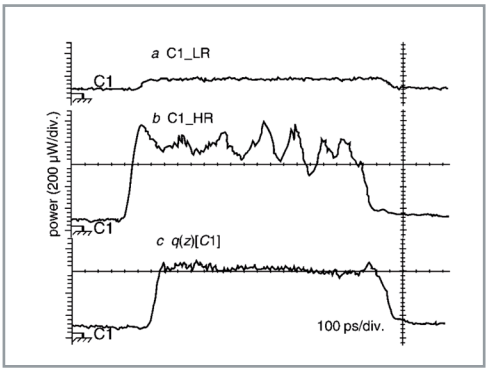

Figure 12. *Encoded signal (impulse response)*

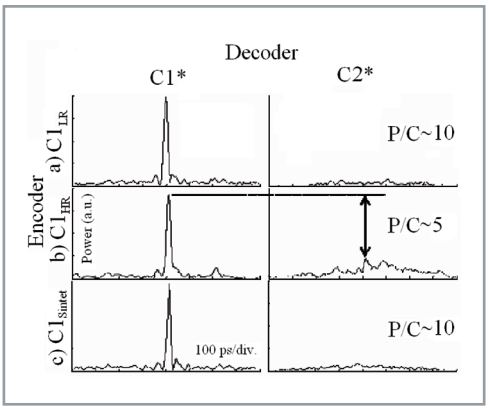

Figure 13. *Encoding=decoding results for C1 LR, HR and q(z)[C1]*

0.6 mm. The whole process was accomplished at constant UV power and exposure time to avoid induced chirp, and the chip amplitude and phase were controlled uniquely by phase control of a double exposure. The complex $q(z)[C1]$ was almost perfectly described by 334 double UV beam exposures (63 exposures spaced 0.6 mm and 271 spaced 0.3 mm), covering the total 119.1 mm device length. Additionally, uniform amplitude devices (standard approach) with weak and strong index perturbations were also fabricated for comparison. Fig. 12 shows the encoded signal (impulse response) for all the devices.

A mode-locked laser (MLL) providing pulses of 3 ps width at 1.25 GHz was applied to the devices. The reflected signal was detected and measured by a 30 GHz bandwidth sampling oscilloscope. The weaker standard device with $|q|{\sim}0.18\ cm^{-1}$ (called LR) in Fig. 12a presents a flat encoded signal without power depletion. This is the better case for encoding/decoding but the peak reflectivity measured was only -8 dB. Fig 12b shows the response for strong devices with $|q|{\sim}1.44\ cm\_1$ (called HR) that provides a peak reflectivity of -2 dB but with a quite damaged encoded profile. Finally Fig. 12c shows the synthesised device with a near flat response and providing a -3 dB peak reflectivity, which indicates a reduction of 5 dB in the insertion loss compared to the weak encoder but maintaining the encoding/decoding capability unaltered. To verify this, we carried out an encoding/decoding experiment. First, pulses were encoded with the LR device based on C1 codeword (LR C1) and decoded consecutively with the corresponding LR matched device (LR C1*) to obtain the autocorrelation peak and then with an orthogonal codeword (LR C2*) from the same 63 Gold-codes family as in [23] to obtain the crosscorrelation measure (Fig. 13a).

Autocorrelation peak (P) against crosscorrelation peak (C) ratio was P/C=10. We substitute the LR encoder by the HR one repeating the decoding with LR C1* and LR C2* (Fig.13b). Now the P/C ratio decreases by 50%, which on average represents a 3 dB increase of interfering power. Finally $q(z)[C1]$ is employed as encoder and the ratio P/C retrieves its original value, but with the outlined improvement in the insertion loss for one device.

5. Conclusions

In this paper we presented a noise and BER modeling, providing simple and intuitive noise power and Q factor expressions for both OOK and DPSK coherent DS-OCDMA systems. Moreover we described into detail the coding-decoding process of coherent Direct Sequence OCDMA devices based on SSFBGs under conditions of non-perfect central wavelength matching and its experimental demostration. Finally we have proposed and demonstrated experimentally a design procedure based on the DLP synthesis method for the SSFBG to be employed in coherent DS-OCDMA systems. Experimental results show that up to 5 dB reduction on insertion losses per device can be obtained maintaining the proper en/decoding capabilities.

References

[1] P.R. Prucnal, M. Santoro and Fanet Ting, "Spread spectrum fiber-optic local area network using optical processing," J. Lightw. Technol. vol 4, no 5, pp. 547–554, May 1986.

[2] J. A. Salehi, "Code division multiple-access technique in optical fiber networks. I. Fundamental principles," IEEE Trans. Commun., vol 37, no 8, pp. 824 – 833, Aug. 1989.

[3] J. A. Salehi and C. A. Brackett, "Code division multiple-access technique in optical fiber networks. II. Systems performance analysis," IEEE Trans. Commun., vol 37, no 8, pp. 834 – 842, Aug. 1989.

[4] K. I. Kitayama, "Code division multiplexing lightwave networks based upon optical code conversion," J. Select. Areas Commun., vol 16, no 7, pp. 1209–1319, Sept. 1998.

[5] Xu Wang and Naoya Wada., "Experimental Demonstration of OCDMA Traffic Over Optical Packet Switching Network With Hybrid PLC and SSFBG En/Decoders," J. Lightw. Technol., vol 24, no 8, pp. 3012-3020, Aug 2006.

[6] Kavehrad, M. & Zaccarin, D. "Optical code-division-multiplexed systems based on spectral encoding of noncoherent sources" Lightwave Technology, Journal of, Vol 13, March 1995, pp.534-545

[7] Hernandez, V.; Mendez, A.; Bennett, C.; Gagliardi, R. & Lennon, W. "Bit-error-rate analysis of a 16-user gigabit ethernet optical-CDMA (O-CDMA) technology demonstrator using wavelength/time codes", Photonics Technology Letters, IEEE, vol 17, Dec 2005, pp. 2784-2786

[8] Zhi Jiang, Dongsun Seo, Shangda Yang, D.E. Leaird, R.V. Roussev, C. Langrock, M.M. Fejer and A.M. Weiner., "Four-User 10-Gb/s Spectrally Phase-Coded O-CDMA System Operating at 30 fJ/bit," IEEE Photon. Technol. Lett., vo 17, no 3, pp. 705- 707, March 2005.

[9] Petropoulos, P.; Wada, N.; Teh, P.; Ibsen, M.; Chujo, W.; Kitayama, K. & Richardson, D. Demonstration of a 64-chip OCDMA system using superstructured fiber gratings and time-gating detection Photonics Technology Letters, IEEE, vol 13, Nov. 2001, pp. 1239-1241

[10] Chen, L. & Smith, P. Demonstration of incoherent wavelength-encoding/time-spreading optical CDMA using chirped moire gratings Photonics Technology Letters, IEEE, vol 12, Sept. 2000, pp. 1281-1283

[11] Cincotti, G.; Wada, N. & Kitayama, K. Characterization of a full encoder/decoder in the AWG configuration for code-based photonic routers-part I: modeling and design Lightwave Technology, Journal of, 2006, Vol 24, pp. 103-112

[12] Agarwal, A.; Toliver, P.; Menendez, R.; Banwell, T.; Jackel, J. & Etemad, S. Spectrally Efficient Six-User Coherent OCDMA System Using Reconfigurable Integrated Ring Resonator Circuits Photonics Technology Letters, IEEE, Vol 18, Sept. 2006, pp. 1952-1954.

[13] T. Hamanaka, Xu Wang, Naoya Wada, A. Nishiki, K. Kitayama, "Ten-User Truly Asynchronous Gigabit OCDMA Transmission Experiment With a 511-Chip SSFBG En/Decoder," J. Lightw. Technol., vol 24, no 1, pp.98-102, Jan. 2006.

[14] Hill, K. O.; malo, B.; Bilodeau, F. & Albert, J. Bragg gratings fabricated in monomode photosenitive optical fibre by UV exposure trough a phase mask App. Phys. lett, Vol 62, 1993, pp. 1035-1037

[15] Xu Wang and K. Kitayama, "Analysis of Beat Noise in Coherent and Incoherent Time-Spreading OCDMA", J. Lightw. Technol., vol 22, no 10, pp. 2226–2235, Oct. 2004.

[16] Amaya, W.; Pastor, D. & Capmany, J. Modeling of a Time-Spreading OCDMA System Including Nonperfect Time Gating, Optical Thresholding, and Fully Asynchronous Signal/Interference Overlapping Lightwave Technology, Journal of, 2008, vol 26, pp. 768-776

[17] J.H. Lee, P.C. Teh, Z. Yusoff, M. Ibsen, W. Belardi, T.M. Monro and D.J. Richardson, "A Holey Fibre-based Nonlinear Thresholding Device for Optical CDMA Receiver Performance Enhancement," IEEE Photon. Technol. Lett., vol 14, no 6, pp. 876-878, June 2002.

[18] H. Sotobayashi, W. Chujo and K. Kitayama., "1.6-b/s/Hz 6.4-Tb/s QPSK-OCDMA/WDM (4 OCDM x 40 WDM x 40Gb/s) Transmission Experiment Using Optical Hard Thresholding", IEEE Photon. Technol. Lett., vol 14, no 4, pp. 555-557, April 2002.

[19] H. Sotobayashi, W. Chujo, and K. Kitayama, "Highly spectral efficient optical code division multiplexing transmission system," IEEE J-ST Quant. Electron., vol. 10, no. 2, pp. 250-258, March-April 2004.

[20] X. Wang, N. Wada, T. Miyazaki, G. Cincotti, K. Kitayama, "Field Trial of 3-WDM × 10-OCDMA × 10.71-Gbps, Asynchronous, WDM/DPSK-OCDMA Using Hybrid E/D Without FEC and Optical Thresholding," J. Lightw. Technol., vol. 25, no. 1, pp. 207-215. Jan. 2007.

[21] X. Wang, N. Wada, T. Miyazaki, and K. Kitayama, "Coherent OCDMA system using DPSK data format with balanced detection,"IEEE Photon. Technol. Lett., vol. 18, no. 7, pp. 826-828, Apr. 2006.

[22] Pastor, D.; Amaya, R. & S., S. Coherent direct sequence optical code multiple access encoding-decoding efficiency versus wavelength detuning Optics Letters, 2007, Vol 32, pp. 1896-1898

[23] Teh, P. C.; Petropoulos, P.; Ibsen, M. & Richardson, D. A comparative study of the performance of seven- and 63-chip optical code-division multiple-access encoders and decoders based on superstructured fiber Bragg gratings Lightwave Technology, Journal of, 2001, Vol 19, pp. 1352-1365

[24] P. C. Teh, M. Ibsen, J. H. Lee, P. Petropoulos and D. J. Richardson, "Demonstration of a Four-Channel WDM/OCDMA System Using 255-Chip 320-Gchip/s Quaternary Phase Coding Gratings," IEEE Photon. Technol. Lett., vol 14, no 22, pp. 227-229, Feb. 2002.

[25] Wang Xu, A. N. N. W. & Kitayama, K. High reflectivity superstructured FBG for coherent

optical code generation and recognition Optical Express, 2004, vol 12, pp. 5457-5468
[26] Pastor, D.; Amaya, W. & Garcia-Olcina, R. "Design Of High Reflectivity Superstructured Fbg For Coherent Ocdma Employing Synthesis Approach", Electronics Letters, 2007, Vol 43, pp. 824 – 825
[27] Skaar, J.; Wang, L. & Erdogan, T. On the synthesis of fiber Bragg gratings by layer peeling Quantum Electronics, IEEE Journal of, 2001, vol 37, pp. 165-173

Biographies

Jose Capmany was born in Madrid, Spain, on December 15, 1962. He received the Ingeniero de Telecomunicacion and the Ph.D. degrees from the Universidad Politécnica de Madrid, Madrid, Spain, in 1987 and 1991, respectively. From 1988 to 1991, he worked as a Research Assistant at the Departamento de Tecnologia Fotonica, Universidad Politécnica de Madrid. In 1991, he moved to the Departamento de Comunicaciones, Universidad Politecnica de Valencia, Valencia, Spain, where he started the activities on optical communications and photonics, founding the Optical Communications Group. He has been an Associate Professor from 1992 to 1996, and Full Professor in optical communications, systems, and networks since 1996. In parallel, he has been Telecommunications Engineering Faculty Vice-Dean from 1991 to 1996, and Deputy Head of the Communications Department since 1996.

Since 2002, he is the Director of the ITEAM Research Institute, Universidad Politécnica de Valencia. His research activities and interests cover a wide range of subjects related to optical communications including optical signal processing, ring resonators, fiber gratings, RF filters, SCM, WDM, and CDMA transmission, wavelength conversion, optical bistability and more recently quantum cryptography and quantum information processing using photonics. He has published over 270 papers in international refereed journals and conferences.

Prof. Capmany has been a member of the Technical Programme Committees of the European Conference on Optical Communications (ECOC), the Optical Fiber Conference (OFC), the Integrated Optics and Optical Communications Conference (IOOC), CLEO Europe, and the Optoelectronics and Communications Conference (OECC). He has also carried out activities related to professional bodies and is the Founder and current Chairman of the LEOS Spanish Chapter, and a Fellow of the Optical Society of America (OSA) and the Institution of Electrical Engineers (IEE). He has acted as a reviewer for over 25 SCI journals in the field of photonics and telecommunications. He is the recipient of the Extraordinary Doctorate Prize of the Universidad Politecnica de Madrid in 1992 and is a Member of the Editorial Board of Fiber and Integrated Optics, Microwave and Optical Technology Letters, and the International Journal of Optoelectronics. He has also been a Guest Editor for the IEEE JOURNAL OF SELECTED TOPICS IN QUANTUM ELECTRONICS.

Waldimar Amaya was born in Bogotá, Colombia. He received the Electronics Engineer, Mobile Telecommunications specialist, and M.Sc. degree from the Distrital University in 1999, 2000 and 2006 respectively. For two years he worked in a HFC CATV operator. Later he was assistant lecturer at Santo Tomas University and Distrital University in Colombia. In 2005 he joined the Optical and Quantum Communications Group (OQCG) where he has worked for 4 years. He received his Ph.D. degree in Telecommunications in the Universidad Politecnica de Valencia, Spain in 2008. Nowadays He is working with OQCG in different projects related with quantum communications.

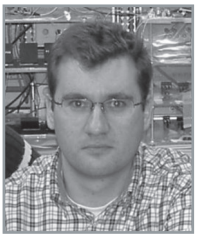

Daniel Pastor, was born in Elda, Spain. He received the Ingeniero de Telecomunicacion degree in 1993 and the Doctor Ingeniero de Telecomunicacion degree (Ph.D.) in 1996, from the Universidad Politécnica de Valencia (UPV), Spain. From 1994 to 1998 he was a Lecturer at the Telecommunications Engineering Faculty and he became an Associate Professor since 1999. He is co-author of more than 120 papers in journals and international conferences in the fields of Optical Delay Line Filters, Fiber Bragg Gratings, Microwave Photonics, WDM and SCM ligthwave systems. He has been leader of 2 national projects, related with Metro and Access optical Networks and Optical Code Division Multiple Access (OCDMA) respectively, and he has been leader of particular work packages in IST European Projects -LABELS (Ligthwave Architectures for the processing of Broadband Electronics Signals), and GLAMOROUS (Glass-based modulators, Routers and Switches) - His current technical interests include Microwave Photonics, Complex Fiber Bragg Grating Fabrication for optical signal processing applications, WDM-SCM networks, RoF systems, and OCDMA techniques.